AFRL-RZ-WP-TP-2010-2143

HIGHLY LOADED LOW-PRESSURE TURBINE: DESIGN, NUMERICAL AND EXPERIMENTAL ANALYSIS (Preprint)

J.P. Clark, P.J. Koch, and S.L. Puterbaugh

Turbine Branch
Turbine Engine Division

J.T. Schmitz, S.C. Morris, R. Ma, and T.C. Corke

University of Notre Dame

JUNE 2010
Interim Report

AIR FORCE RESEARCH LABORATORY
PROPULSION DIRECTORATE
WRIGHT-PATTERSON AIR FORCE BASE, OH 45433-7251
AIR FORCE MATERIEL COMMAND
UNITED STATES AIR FORCE

REPORT DOCUMENTATION PAGE

Form Approved
OMB No. 0704-0188

1. REPORT DATE *(DD-MM-YY)*	2. REPORT TYPE	3. DATES COVERED *(From - To)*
June 2010	Conference Paper Preprint	06 June 2008 – 05 June 2010

4. TITLE AND SUBTITLE
HIGHLY LOADED LOW-PRESSURE TURBINE: DESIGN, NUMERICAL AND EXPERIMENTAL ANALYSIS (Preprint)

5a. CONTRACT NUMBER
IN HOUSE

5b. GRANT NUMBER

5c. PROGRAM ELEMENT NUMBER
62203F

6. AUTHOR(S)
J.P. Clark, P.J. Koch, and S.L. Puterbaugh (Turbine Engine Division, Turbine Branch (AFRL/RZTT))
J.T. Schmitz, S.C. Morris, R. Ma, and T.C. Corke (University of Notre Dame)

5d. PROJECT NUMBER
3066

5e. TASK NUMBER
06

5f. WORK UNIT NUMBER
306606W8

7. PERFORMING ORGANIZATION NAME(S) AND ADDRESS(ES)

Turbine Branch (AFRL/RZTT)
Turbine Engine Division,
Air Force Research Laboratory, Propulsion Directorate
Wright-Patterson Air Force Base, OH 45433-7251
Air Force Materiel Command
United States Air Force

University of Notre Dame
Dept. of Aerospace and
Mechanical Engineering

8. PERFORMING ORGANIZATION REPORT NUMBER
AFRL-RZ-WP-TP-2010-2143

9. SPONSORING/MONITORING AGENCY NAME(S) AND ADDRESS(ES)

Air Force Research Laboratory
Propulsion Directorate
Wright-Patterson Air Force Base, OH 45433-7251
Air Force Materiel Command
United States Air Force

10. SPONSORING/MONITORING AGENCY ACRONYM(S)
AFRL/RZTT

11. SPONSORING/MONITORING AGENCY REPORT NUMBER(S)
AFRL-RZ-WP-TP-2009-2143

12. DISTRIBUTION/AVAILABILITY STATEMENT
Approved for public release; distribution unlimited.

13. SUPPLEMENTARY NOTES
PAO Case Number: 88 ABW-2009-5169; Clearance Date: 10 December 2009. ©2010 ASME. The U.S. Government is joint author of the work and has the right to use, modify, reproduce, release, perform, display, or disclose the work. To be presented at the ASME Turbo Expo: Power for Land, Sea, and Air, June 14-18, 2010, Glasgow, Scotland. Paper contains color.

14. ABSTRACT
The performance and detailed flow physics of a highly loaded, transonic, low-pressure turbine stage has been investigated numerically and experimentally. The mean rotor Zweifel coefficient was 1.35, with a work coefficient of 2.8, and a total pressure ratio of 1.75. The aerodynamic design was based on recent developments in boundary layer transition modeling. Steady and unsteady numerical solutions were used to design the blade geometry as well as to predict the design and off-design performance. Measurements were acquired in a recently developed, high-speed, rotating turbine facility. The nozzle-vane only and full stage characteristics were measured with varied mass flow, Reynolds number, and free-stream turbulence. The efficiency calculated from torque at the design speed and pressure ratio of the turbine was found to be 90.6%. This compared favorably to the meanline target value of 90.5%. This paper will describe the measurements and numerical solutions in detail for both design and off-design conditions.

15. SUBJECT TERMS
turbomachinery, turbines, high lift airfoils, high work turbines

16. SECURITY CLASSIFICATION OF:			17. LIMITATION OF ABSTRACT:	18. NUMBER OF PAGES	19a. NAME OF RESPONSIBLE PERSON (Monitor)
a. REPORT	b. ABSTRACT	c. THIS PAGE			Dr. John Clark
Unclassified	Unclassified	Unclassified	SAR	20	19b. TELEPHONE NUMBER *(Include Area Code)* N/A

Standard Form 298 (Rev. 8-98)
Prescribed by ANSI Std. Z39-18

Proceedings of GT2010
ASME TURBO EXPO: Power for Land, Sea, and Air
June 14-18, 2010, Glasgow, Scotland

DRAFT GT2010-23591

HIGHLY LOADED LOW-PRESSURE TURBINE: DESIGN, NUMERICAL, AND EXPERIMENTAL ANALYSIS

J. T. Schmitz, S. C. Morris*, R. Ma, and T. C. Corke
Dept. of Aerospace and Mechanical Engineering
University of Notre Dame
Notre Dame, IN, USA
Email: s.morris@nd.edu

J. P. Clark, P. J. Koch, and S. L. Puterbaugh
Propulsion Directorate
Air Force Research Laboratory
Building 18, Room 136D
1950 5th St., WPAFB, OH 45433 USA
john.clark.38@us.af.mil

ABSTRACT

The performance and detailed flow physics of a highly loaded, transonic, low-pressure turbine stage has been investigated numerically and experimentally. The mean rotor Zweifel coefficient was 1.35, with $dh/U^2 = 2.8$, and a total pressure ratio of 1.75. The aerodynamic design was based on recent developments in boundary layer transition modeling. Steady and unsteady numerical solutions were used to design the blade geometry as well as to predict the design and off-design performance. Measurements were acquired in a recently developed, high-speed, rotating turbine facility. The nozzle-vane only and full stage characteristics were measured with varied mass flow, Reynolds number, and free-stream turbulence. The efficiency calculated from torque at the design speed and pressure ratio of the turbine was found to be 90.6%. This compared favorably to the meanline target value of 90.5%. This paper will describe the measurements and numerical solutions in detail for both design and off-design conditions.

NOMENCLATURE

b_x Rotor Axial Chord
v_x Vane Axial Chord
c_p Specific heat at constant pressure
Zw Incompressible Zweifel load coefficient
Re Reynolds number (inlet conditions and true chord)
η Efficiency
h Enthalpy
U Rotor Velocity
A Area
N Rotor Speed (rpm)
Tu Turbulence Intensity
$P_{t,in}$ Total inlet pressure
$T_{t,in}$ Total inlet temperature
ND Notre Dame
HiLT Highly Loaded Turbine

INTRODUCTION

Most modern gas-turbine engines utilize a multi-shaft design with a separate high pressure turbine and low pressure (LP) turbine. The LP turbine is often used to power a low-pressure compressor and/or fan in the case of a turbo-fan engine, or can be directly connected to a rotor-drive for rotary-wing and power applications. The LPT is therefore an important component in the determination of the overall engine performance and efficiency. Current LP turbines operate with efficiencies above 90%, and so continued increases in efficiency through better aerodynamic design are difficult to obtain [1].

The LPT often has a large diameter in order to obtain the maximum possible power at a fixed rotational speed. As a result, the weight of the LPT can be up 30 percent of the total weight of an aircraft engine [2], and may contain as many as

*Address all correspondence to this author.

2000 individual airfoils [3]. A NASA system study showed that a 10% reduction in the weight of the LP turbine is more effective than any other engine component at reducing the Direct Operating Cost plus Interest (DOC+I) of an engine on a large transport aircraft [4]. Consequently, the focus of significant LP turbine research has been directed towards improving engine design through weight reduction.

System life-cycle costs rise in tandem with turbine weight and part count. The weight and part count of an LP turbine is affected by two parameters. The first is the work output per stage, $\Psi = dh_T/U^2$ where dh_T is the total enthalpy change across the stage, and U is the mid-span blade velocity. At a given size and wheel speed, increasing the Ψ value can lower the number of required LP turbine stages. The second parameter is the blade loading as defined by the incompressible Zweifel coefficient:

$$Zw = 2\frac{\tau}{b_x}cos^2\beta_2(tan\beta_1 + tan\beta_2) \quad (1)$$

where τ is the airfoil pitch, b_x is the axial chord, and β_1 and β_2 are the inlet and exit flow angles, respectively. Increasing the Zw value lowers the number of blades per stage while maintaining the same work output. Thus, both Ψ and Zw can be used to reduce the weight of the LP turbine section. However, these changes lead to an increase in the aerodynamic loading of each blade. This generally results in higher overall losses which can lead to a decrease in the stage efficiency of "highly loaded" designs. These issues are often of greatest concern at low Reynolds number that occurs in flight at cruise conditions. The low Reynolds number flow present in LP turbines at high altitudes often results in significant regions of laminar flow on the suction side of the airfoils, which makes them susceptible to laminar separation which may or may not reattach [5]. Despite the challenges presented by highly loaded designs, progress has been made during the past two decades towards the reduction of LP turbine blade counts, and a brief summary follows.

The aerodynamics of highly loaded LP turbines was studied by Hoheisel et al. [6]. A family of cascade airfoils were developed with the designation T104 - T106. These airfoils included both front and aft loading with Zw values ranging from 1.04 to 1.07. These and related airfoils have been used in cascade investigations by the research groups of both Hodson [7] and Fottner [8].

Haselbach et al. [9] presented a high-lift LP turbine design that was specific to the BR715 engine. The authors reported an increase in the measured performance differential between take-off and cruise conditions that was attributed to increased endwall losses. In a similar work, Gier and Ardey [10] reported on the use of CFD-based transition modeling to design high-lift airfoils for a three-stage LP turbine rig. The authors applied aft loading to their high-lift designs and found that measured performance was lost more rapidly with decreasing Reynolds number compared to the conventional-lift design. This degradation in performance was attributed to boundary layer separation on the airfoil surfaces.

Prakash et al. [11] reported on the effect of loading level and distribution (front, mid and aft) on LP turbine profile losses. The data demonstrated increased suction side separation and high losses as the loading level increases, the loading is moved aft or the Reynolds number decreases. Although secondary loss was not addressed by the authors, they did comment that front loaded blades typically have lower profile losses but higher secondary losses.

An important series of experiments that focussed on high work LPT stages was funded by NASA at General Electric in the 1970s and 80s. These include the multi-stage fan-drive turbine of Evans and Wolfmeyer [12] and the 5-stage E^3 LPT of Cherry and Dengler [13] that had average work coefficients of 3.0 and 2.66 per stage, respectively. Both studies achieved efficiencies near 90%, albeit with more conventional-lift airfoils with incompressible Zweifel coefficients of order 1.

Recently, Bons et al. [14] tested a new cascade airfoil design, designated L1M, with $Zw = 1.34$. This airfoil was designed with integrated flow control in anticipation that the high-lift design would require some form of separation control. However, the airfoil proved to perform well without the activation of the flow control. The most highly loaded LP airfoil reported in the open literature appears to be that designed and investigated by Praisner et al. [3]. The authors tested airfoils with Zweifel coefficients of 1.62 and 1.82.

While considerable success with high-lift LPT airfoils was demonstrated in many of the above studies, especially for incompressible cascades, other recent work argues for maintaining loading levels at more modest levels. Coull et al. [15] performed exceptionally detailed measurements of flat plate boundary layers under adverse pressure gradient conditions that simulated airfoils with Zweifel coefficients that were no larger than that of Pack B (1.15). Also, Gier et al. [16] argued strongly that the optimum LPT lift level occurs when $0.8 < Zw < 1.0$. Anecdotal information recently appeared in Aviation Week [17, 18] stating that attempts at reducing part count in large commercial LPTs have met with disappointment.

The current study was motivated by the need to understand the apparent inconsistency that exists between the successful high-lift cascade experiments (e.g. [3, 11, 14]) and the less successful attempts in engines [17, 18]. The objective/goal of the present research was to design and demonstrate a high-work, highly-loaded airfoil design that maintained a high efficiency. The design outcome was a transonic turbine stage designated the Notre Dame Highly Loaded Turbine 01, (ND-HiLT01). The stage has a mean rotor Zweifel coefficient of 1.35, a work coefficient of $dh/U^2 = 2.8$, and a measured stage efficiency of $\eta = 90.6\%$. The experimental turbine design is consistent with

both a reduction in stage count in a gas turbine engine and a decrease in the part count of an individual airfoil row. The test data presented here provide further validation of the transition modeling system presented by Praisner and Clark [19] and Praisner et al. [20] since the same design, analysis, and modeling techniques used to design previous airfoils (See e.g. [14]) were used here. That is, the modeling techniques used previously for incompressible cascades have been demonstrated adequate in a rotating, compressible environment. The following sections will outline the design process, both steady and unsteady CFD results, and a complete set of experimental measurements for the ND-HiLT01 obtained in a high-speed rotating turbine rig.

LOW PRESSURE TURBINE STAGE DESIGN

The ND-HiLT01 geometry design was based on a turbine design loop that is described in detail by Clark et al. [21] and illustrated in Fig. 1. Initially, engine cycle data were used to set the basic parameters for the turbine (i.e. pressure ratio, rotational speed, and power requirements). These were used to define stage velocity triangles through a 1D meanline design and analysis tool developed by Huber (described in more detail in [21]). The 2D airfoil profiles were created via a shape generation algorithm also described by Huber [21] and analyzed with 2- and 3-D RANS calculations. Design-optimization techniques were used at the profile-definition level to achieve a low-loss design. The design loop was iterative, so a return to a less rigorous level of analysis was possible as design changes were made. The current stage required 12 iterations through the analysis.

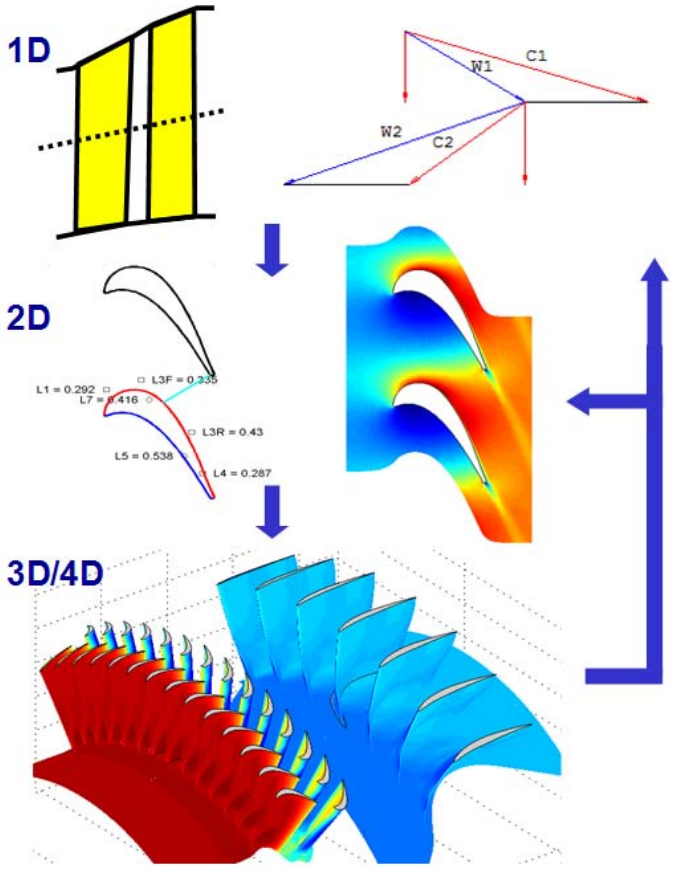

Figure 1. Turbine design loop used to define the ND-HiLT01 stage.

Cycle Requirement and Design Velocity Triangles

The turbine stage basic cycle parameters are shown in Table 1. The work coefficient was initially set to be 2.8, which can be considered high relative to a state-of-the-art large commercial engine. This led to a high degree of blade turning and a target efficiency level that was slightly above ninety percent. These design targets were set mainly through considerations of the overall goal of the program: to demonstrate acceptable aerodynamic performance, if possible, while reducing the effective part count of a notional LPT.

To set the design velocity triangles of the machine, the meanline trade space was explored considering the wheel speed, airfoil Zweifel coefficients, and stage reaction. A shrouded stage was designed and trailing-edge diameters and airfoil taper ratios were set to constant levels that were consistent with state-of-the-art turbines. Since the main research goal of the stage was to determine whether it was possible to achieve a high-lift (i.e. low airfoil count) rotating airfoil design without sacrificing stage performance, it was decided to place all aerodynamic technology in the blade row only with the vane row having modest design goals. So, while the Zweifel coefficient of the blade row was set to a level of 1.35, the vane row was set to 0.89 (near the optimum defined by Gier et al [16]).

2D Profile Design, Analysis, and Optimization

Airfoil shapes for the stage were designed to meet meanline turning requirements using the profile generator of Huber (again, see [21]). The algorithm was similar to one described by Casey [22] in that it used Bezier curves in conjunction with typical leading- and trailing-edge specifications (e.g. wedge angles, edge radii of curvature, gage areas, and uncovered turning) to define airfoil shapes using a small number of control points. Once the profile was defined, the grid generator and RANS solver described by Dorney and Davis [23] were used along with an ad hoc implementation of the transition models of Praisner and Clark [19] to determine airfoil performance. Graphical User Interfaces (GUI) were employed to alter the specification of the airfoil shape as well as parameters used to define both the generation of the grid and the operation of the flow solver. In addition, design optimization (Sequential Quadratic Programming, SQP [24]) and design-of-experiments techniques (Latin hyper-

Table 1. Meanline Design Parameters for ND-HiLT01

Parameter	Vane	Blade	Stage
$T_{t,in}$ K	358	—	—
$P_{t,in}$ kPa	97.9	—	—
Inlet Flow Param. $[\frac{(kg/s)K^{1/2}}{kPa}]$	0.957	—	—
Corrected Flow (kg/s)	5.71	—	—
Work Coefficient $[\frac{\Delta h}{U^2_{mean}}]$	—	2.80	—
Energy Function $[\frac{J}{kgK}]$	—	134	—
Flow Coefficient $[\frac{C_{x,exit}}{U_{mean}}]$	—	0.78	—
Efficiency	—	—	90.5
Pressure Ratio (total-total)	—	—	1.75
Reaction (%)	—	—	38
$\frac{N}{T^{1/2}_{t,in}}$ (rpm/$K^{1/2}$)	—	332	—
Corrected Speed (rpm)	—	5630	—
AN^2x10^{-6} (m rpm)^2	—	3.35	—
Exit Mach Number	0.76	0.78 (rel)	—
Airfoil Count	60	70	—
Zweifel Coefficient	0.88	1.35	—
Overall Turning (deg)	96	123	—
Gas Angle (deg) (inlet/exit)	26.7/69.6	54.7/67.8	49.5

cube sampling [25]) were used to define low-loss profiles with acceptable loading distributions. Each airfoil was designed as a set of 2D profiles at radii equal to the root, midspan, and tip locations in the flowpath. The blade shape was also designed at 25% and 75% of span. In the course of stage design, more than 3500 candidate profiles were analyzed at the 2-D RANS level in order to achieve the final geometry.

Previous High-Lift Cascade Airfoils. The profile design of the stage considered the results of several previous cascade studies. Specifically, a recently developed family of LP turbine airfoils were designed to study low Reynolds-number, high-lift aerodynamics. Several profiles of these previous designs as well as the ND-HiLT01 profile are shown in Fig. 2. Like the current stage profiles, all airfoils were designed with a combination of GUI-driven design iterations and optimization techniques. All of the geometries shown were derived using the transition modeling studies of Praisner and Clark [19]. Additionally, all the airfoils have velocity triangles in keeping with the Pratt & Whitney Pack B geometry. A pair of airfoils was designed to an incompressible Zweifel coefficient of 1.34, and these airfoils differed markedly in the loading convention used for the respective designs. The first airfoil, dubbed the L1M (level one increase in lift, mid-loaded), was shown by Bons et al. [14] to have a significantly better loss characteristics at low Reynolds number compared to the Pack B airfoil, while having 17% higher loading. The airfoil was also used by Gross and Fasel [26] as well as Bons et al. [27] to assess the physics of flow control for such a high-lift airfoil.

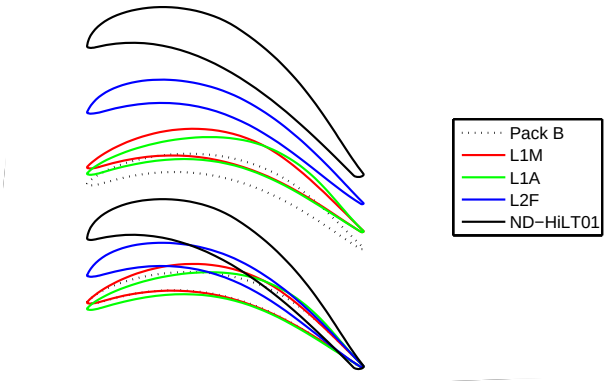

Figure 2. A family of high lift LPT airfoils designed at AFRL, as compared to the Pack B and ND-HiLT01 profile.

More recently another airfoil called the L1A (aft-loaded) was designed to the same pitch-to-chord ratio as the L1M, and it has been studied at several universities under the NASA Fundamental Aeronautics Program [e.g. [28], [29]] by researchers working on various aspects of low Reynolds-number LPT flows and/or flow control in highly-loaded LPTs. Whereas the L1M airfoil had an exceptionally good Reynolds-lapse characteristic, the L1A airfoil was designed to have a significant degradation in performance at low Reynolds numbers. The L1A is therefore a much better platform for the study of flow-control physics than the L1M. Additionally, because it is more aft-loaded the impact of the high lift level on secondary losses is expected to be reduced relative to that of the L1M.

The final cascade geometry designed with the current system and tested is the L2F airfoil of McQuilling [29]. The L2F is more front-loaded than either the L1M or the L1A airfoils, and it has 39% greater lift than the Pack B airfoil at high Reynolds numbers. This airfoil was designed to test the limits of high lift, low Reynolds-number operation enabled by increases in transition

modeling fidelity. As predicted, the airfoil did have improved lapse characteristics over the Pack B, even at this extreme level of loading.

The mass-averaged loss coefficient for the entire family of airfoils is shown in Fig. 3 as a function of Reynolds number. Both the measured and predicted variations are shown, and these are compared against the Pack B for reference. All predictions were made in advance of testing in low speed cascades at AFRL [29] and the Ohio State University [28]. The predictions were made within the design and analysis system, and the transition was modeled using only the separated-flow transition model of Praisner and Clark [19]. The predictions were therefore somewhat conservative in that transition may occur in the experiment prior to separation, depending upon the level of freestream turbulence applied in the experiments. What is most important for the designer is a high level of confidence in the predictions of boundary layer separation, transition, and re-attachment at both design and off-design conditions. The pre-test predictions presented in Fig. 3 demonstrate that these features are adequately modeled in the present design system.

The predicted loss coefficient vs. Reynolds number for the ND-HiLT01 design is also shown in Fig. 3. The values suggest an increase in total pressure loss compared to the cascade airfoils at the higher Reynolds number as might be anticipated given the profiles shown in Fig. 2. The ND-HiLT01 blade has a much larger level of turning compared to the previous cascade airfoils. This is consistent with both the high level of work coefficient and the increase in high Reynolds number loss over the previous airfoils. However, only a modest increase in loss is observed at low Reynolds number.

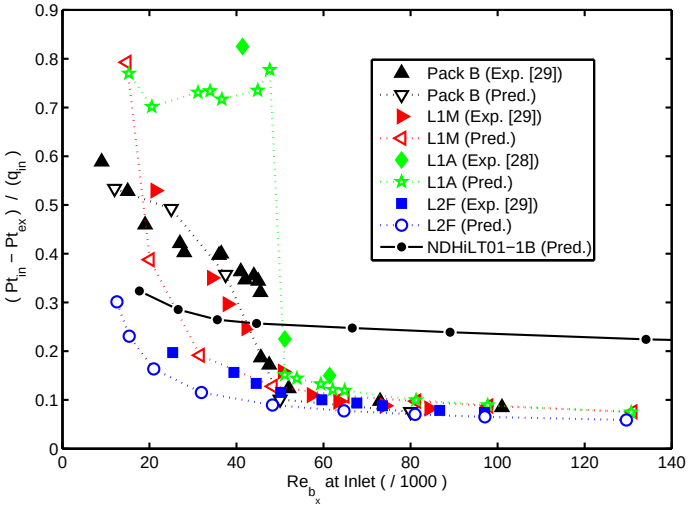

Figure 3. Mass averaged losses as a function of Reynolds number for the family of airfoils designed at AFRL along with Pack B variation and the ND-HiLT01 geometry.

3D Airfoil Stacking and Analysis

The 2D airfoil profiles were designed at root-, mid-, and tip radii, and then stacked radially to define 3D geometries [30]. Additionally, spline fits were made to values of airfoil profile inputs, and these were used to define 25% and 75% airfoil sections as well as to create extrapolated airfoil sections that extend the 3D geometry through the endwalls. An example of two such splined profile parameter variations is shown in Fig. 4. In this way, smooth 3D profiles were assured, and this also aided in 3D grid generation for subsequent RANS analysis. The above process was followed exclusively for the vane row. The blade row required additional 2D design extrapolations at 25% and 75% span to assure that the most effective high-lift profiles were produced. The blade and upstream vane were stacked on profile centroids of area. That is, no further 3D refinement of the geometries was allowed beyond that required at the meanline level. This assured that the turbine design was a true test of high-lift profile design philosophy to achieve acceptable performance at reduced part count/stage weight.

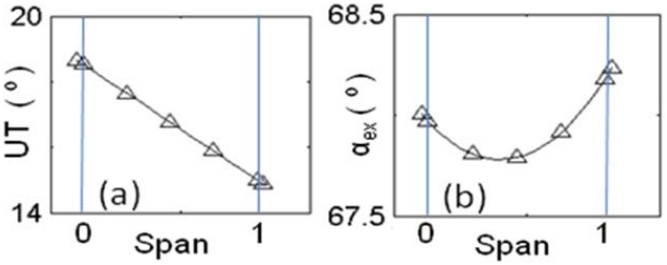

Figure 4. Representative spline fits to profile design parameters (a) uncovered turning and (b) exit air angle (α_{ex}) that were used to define the 3D turbine blade.

The complete design loop was closed through the level of 3D unsteady RANS analysis 12 times throughout the aerodynamic design phase of the LPT stage. These unsteady RANS calculations were all performed with the code of Dorney and Davis [23], and they were executed at quasi-regular intervals as the 2D airfoil profiles were further refined for lower loss and improved loading distribution. Additional design evaluation calculations and pre-test predictions were undertaken with the LEO steady and unsteady RANS solver of Ni [31]. This code is built on Ni's implementation [32] of the Lax-Wendroff algorithm [33], and it has excellent turnaround time for 3D unsteady analyses. A typical 3D steady RANS simulation is converged in under 4 hours of wall clock time, whereas a time-resolved calculation is converged (based on efficiency) in about 4 days. All 3D steady calculations with the Ni code include a mixing-plane between rows, and both time-averaged and time-resolved performance characteristics of the flowfield are discussed below, as warranted.

De-Swirler Airfoil Design Because the turbine designed was consistent with an embedded stage of a multi-row LPT, the flow discharged from the turbine stage was highly skewed, especially near the inner annulus. Also, a significant range in air angle occurred over the span. In order to pass this flow through a set of large struts located less than 2 annulus heights downstream of the turbine, a set of outlet guide vanes was designed. The constraints on the design were that the axial extent of the blade row must be 66 mm or less and the inner and outer annulus walls must remain cylindrical. This design space necessarily resulted in very highly loaded airfoils - particularly near the annulus ID. Fortunately, reducing total pressure loss was not a first order design criteria for this application. The main goal was to reduce the swirl to a level of less than twenty degrees over the entire span at the exit.

To meet this design goal, a streamline curvature code (UD0300M) developed by USAF [34] for compressor airfoils was used to establish initial aerodynamic performance and generate a 3D blade shape. Then, the performance of the airfoil was assessed using 3D unsteady RANS and adjustments to the blade shape were made using UD0300M (See the final airfoil in Fig. 1). NACA 65 series airfoils were employed and radial leading and trailing edges were used to decrease complexity. The spanwise solidity distribution varied from 2.6 at the ID, to 1.8 at midspan, to 1.6 at the OD (35 vanes) and the aspect ratio was approximately 1. The thickness of the airfoils was 7% of chord.

The biggest challenge in the design was handling the secondary flows that resulted from the highly loaded airfoils near the annulus ID. Initial design iterations indicated highly separated flow near the annulus ID on the airfoil suction side, some separation on the suction surface near the leading edge toward the annulus OD, and significant overturning near midspan due to secondary flow. In order to improve the separation near the ID by diverting higher energy flow inward, the vane was tilted circumferentially 15 degrees with the tip moving into the direction of incoming flow. The separation near the OD was improved by increasing the leading edge airfoil thickness to 0.7% of chord. Finally, the overturning near the midspan was reduced by adjusting the deviation model in UD0300M by the amount dictated by the CFD results. Additional performance optimization was possible, but not required for the application.

EXPERIMENTAL FACILITY

The data presented in this paper were obtained from the transonic axial turbine facility at the University of Notre Dame. The facility was designed to accommodate a wide range of turbine stage designs. A diagram of the mechanical and flow layout of the turbine is shown in Figure 5. The turbine is coupled to a shaft that is levitated on active magnetic bearings. During operation the bearing system held the rotor center line to ± 10 microns radially and ± 5 microns axially.The turbine shaft is connected through a torque meter to a speed reducing gearbox. The gearbox output shaft is connected to a variable speed AC motor drive which is connected to a centrifugal compressor. Note that the motor is in a "load-sharing" configuration such that the combination of the turbine power and electrical power are used to drive the compressor.

The flow path is a partial-closed-loop system. The airflow into the turbine is at approximately atmospheric pressure, and a design temperature of 95 degrees Celsius. The turbine exit flow is at sub-atmospheric pressure and nominally room temperature (depending on the design of the turbine). The flow from the turbine enters a settling chamber and a fast acting safety valve. The flow then moves through a Venturi mass flow meter before entering the compressor inlet. The uncertainty in the measured mass flow rate based on error propagation was estimated to be $\pm 0.3\%$, and was found to be repeatable to within $\pm 0.05\%$. The flow then enters the compressor, and exits at roughly atmospheric pressure and elevated temperature. The compressor utilizes variable inlet and exit guide vanes. A portion of this exit air is recycled to the turbine inlet in order to maintain a constant, elevated turbine inlet temperature. A large settling chamber and inlet duct are located just upstream of the test turbine. Further details of the facility are described by Ma et. al [35].

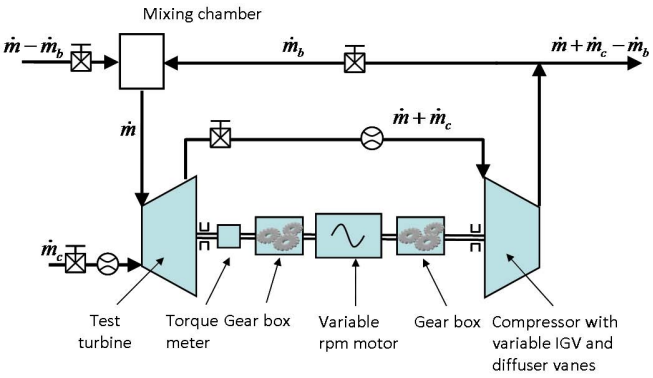

Figure 5. Schematic of the Notre Dame Turbine Facility

The ND-HiLT01 stage described in the previous section was installed into the facility test section. A schematic of the flow cross section is shown in Figure 6. Inlet hub and tip diameters are 0.32m and 0.43m, respectively. The respective rotor exit diameters are 0.33m and 0.47m. The 60 blade nozzle and 70 blade rotor were each machined from solid Aluminum forgings. The rotor design included a shroud with a 5-fin outer rim seal. The fore and aft rim seal cavities were isolated to ensure no rim seal flows were present during testing.

Total pressure Kiel and total temperature rakes were installed $2v_x$ upstream of the stage inlet and $1b_x$ downstream of

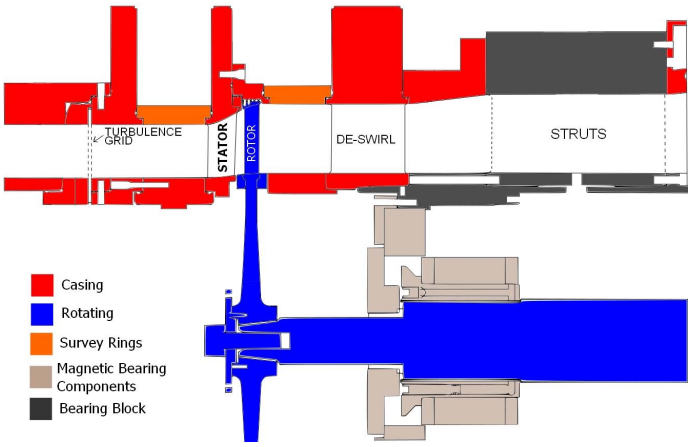

Figure 6. Schematic of the ND-HiLT01 Experimental Setup

the stage exit. There were 6 inlet and 8 exit, equal area spaced sensor locations. The radial position of each sensor was duplicated at a 180 deg offset, for a total of 12 inlet and 16 exit probes. To avoid possible heat transfer from the casing to the rakes, nylon inserts were used to isolate each rake from the aluminum casing. Also, to avoid large inlet thermal boundary layers, an electric coil heating unit preheats the stage inlet casing to match the inlet air temperature. The pressures were measured with an Esterline NetScanner 9816/98RK-1 pressure scanner with an operating range of $\pm$6.9 kPa. The temperature measurements were acquired with a National Instruments CFP-CB-3 Compact Fieldpoint unit, equipped with CFP-TC-120 modules and K-type thermocouples. The reference pressures for the differential measurements were acquired with Setra Model 270 absolute pressure transducers having a range of 0-137.9 kPa. Uncertainties for the total pressure probe measurements due to calibration, linearity, and hysteresis are estimated to be $\pm$0.1% of full scale range, and $\pm$0.4 K for the total temperature.

A removable, perforated plate turbulence grid was installed 89mm upstream of the stage inlet. A single wire hotwire anemometer (AA Lab Systems model AN-1003) was used to measure the freestream turbulence intensity (FSTI). The turbulence scales were computed according to the methods of Bernard and Wallace [36]. The without grid FSTI and integral length scale without the grid were 3.0% and 12mm, respectively. The values with the grid were 5.5% and 8mm.

A Torquetronics ET2350 phase shift torquemeter is installed between the turbine and turbine gearbox. This location, and use of magnetic bearings, allows for a measurement of the turbine torque and speed that does not require modification due to bearing losses. The estimated uncertainty in torque and speed are $\pm$0.1% and $\pm$0.04%, respectively. The power was also estimated using the total temperature measurements and mass flow rate, and assuming adiabatic conditions. These power values agreed to within 0.25%, which provides an estimate for the bias errors that may be present in the measurements. The adiabatic and torque-based efficiency values had an overall estimated uncertainty of $\pm$0.4%. The efficiency values presented later in this paper were derived using the power estimated from the torque and rotational speed.

NOZZLE ANALYSIS

A series of nozzle-only test data were obtained at various Reynolds numbers and two FSTI levels. The intent was to verify the nozzle design and to document the characteristics of the rotor inlet flow. The rotor was removed and replaced with flow path casing parts. A Kiel total pressure probe was then traversed $0.24v_x$ downstream of the nozzle exit. This location is the nominal location of the rotor blades leading edge. The traverse consisted of 21 radial points and 0.5 degree spacing in the azimuthal direction.

The nozzle loss was quantified with a total pressure loss coefficient defined as

$$C_P = \frac{P_{T,CL} - P_{T,exit}}{Q_{CL}} \tag{2}$$

where C_P is the wake loss coefficient, $P_{T,CL}$ is the inlet centerline total pressure, $P_{T,exit}$ is the nozzle exit total pressure and Q_{CL} is the inlet centerline dynamic pressure. These values were area averaged in order to provide the net loss coefficient

$$C_{P,A} = \frac{1}{A}\int \frac{P_{T,CL} - P_{T,exit}}{Q_{CL}} dA \tag{3}$$

These values are shown for both inlet turbulence values as a function of the Reynolds number in Fig. 7. The losses decreased by about $\sim$ 30% as the Reynolds number was increased from 14,000 to 190,000. The values were similar for the two turbulence intensity magnitudes measured, showing only a slight increase in the $C_{P,A}$ value for the Tu=3.0% case at higher Reynolds number. A meanline study was conducted using the nozzle geometry. The results from these calculations are also shown in Fig. 7. The predicted losses were higher overall, but the airfoil did not appear to be susceptible to separation.

Two example contour plots of the wake loss coefficient are shown in the figure inset for the Re = 14,000 and 125,000 cases with Tu=5.5%. The blade wake is well defined in both cases with the lower Reynolds number case showing that the increase in the $C_{P,A}$ value is primarily due to an increase in the width of the wake at the lower Reynolds number. Also, at all Reynolds numbers the majority of the losses were found to be concentrated in the end-wall regions, where local maxima in C_P were observed. These are presumed to be related to the passage vortex structure as described by Langston et al. [37].

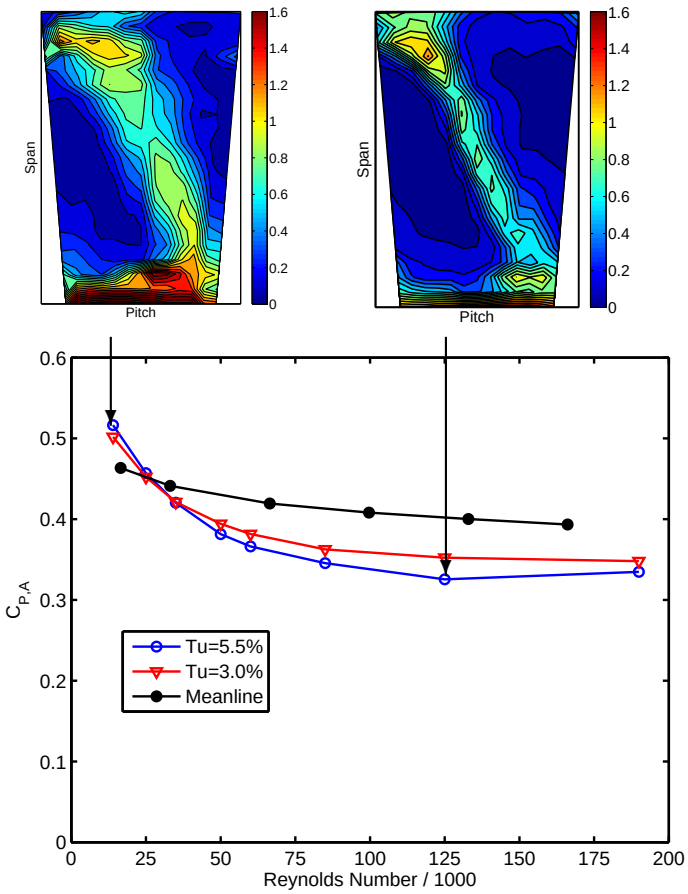

Figure 7. ND-HiLT01 Vane Reynolds-lapse data, exit wake contours, and meanline prediction

ROTOR / STAGE ANALYSIS

Experimental measurements of the ND-HiLT01 stage were acquired at both design and off-design conditions. The data were obtained from $0.50N_c$ to $1.00N_c$, where N_c is corrected speed. At each of six fixed speed values the corrected mass flow rate ($\dot{m}_c$) was varied in order to change the rotor incidence. These experiments were completed with and without the inlet turbulence grid installed which resulted in two values of the inlet turbulence intensity as described above. All measured quantities have been corrected using the equations in Table 2 with P_{ref} 101.33 kPa and T_{ref} = 288.17 K.

The total pressure ratio is shown as a function of the corrected mass flow rate in Fig. 8. The total temperature ratio is shown in a similar format in Fig. 9. The data show an expected monotonic increase in both pressure ratio and temperature ratio with mass flow at each speed. Almost no evidence of changes in performance with FSTI were observed. The slope of the curves increased substantially at the higher mass flow values suggesting choked or nearly choked flow in the rotor (note that the nozzle exit Mach number is 0.8 at the design mass flow).

Table 2. CORRECTED PARAMETERS

	Symbol	Non-Dimensional
Inlet Pressure	P_{Ti}	$\delta = \frac{P_{Ti}}{P_{ref}}$
Inlet Temperature	T_{Ti}	$\theta = \frac{T_{Ti}}{T_{ref}}$
	Symbol	Corrected
Rotational Speed	$N(rpm)$	$N_c = \frac{N}{\sqrt{\theta}}$
Mass flow rate	$\dot{m}$	$\dot{m}_c = \frac{\dot{m}\sqrt{\theta}}{\delta}$

The meanline predictions and design point are plotted in both figures, and show reasonable agreement across the speed range tested. Both the pressure ratio and temperature ratio were over predicted at lower speeds. This suggests that the exit deviation angle was slightly higher than predicted by the meanline code. However, since the meanline model assumes attached flow with minimal effects of boundary layers, the relative agreement suggests that the boundary layers in the turbine rotor are not separated, even at the lower speeds where the Reynolds number was approximately 80,000.

The mass flow at which the rotor becomes choked appears to be slightly over-predicted by the meanline resulting in lower PR and TR values at the highest mass flow values compared to the experimental results. This again is likely due to small differences in boundary layer characteristics and flow deviation which can affect the net through-flow area that is available to the rotor exit flow in the relative reference frame.

The efficiency of the turbine is plotted on a delta basis as a function of the PR in Fig. 10. For both the measurements and the calculations, the efficiency at the design point was used to calculate the delta level. Note that at design there was a 1% difference in measured and predicted efficiency with the calculation lower than the data. This was consistent with the use of fully-turbulent computations to obtain the predicted efficiency. Also, linear trend lines have been added to the $0.90N_c$, $0.95N_c$, and $1.00N_c$ experimental data for both FSTI cases for visual reference. The vertical dashed line corresponds to the design pressure ratio of 1.75. The horizontal dashed line represents the absolute efficiency value of 90.5% that was numerically predicted at the design mass flow rate.

The efficiency at lower speed was generally between 90% and 93%, and was observed to be sensitive to the flow incidence. That is, increased mass flow and pressure ratio resulted in a lower efficiency. The relatively high efficiency values suggest that the airfoil design is insensitive to both Reynolds number and Mach number. Although these parameters were not varied independently with rotor speed only, the blade exit Reynolds number varied from 59k to 120k and the exit Mach number varied

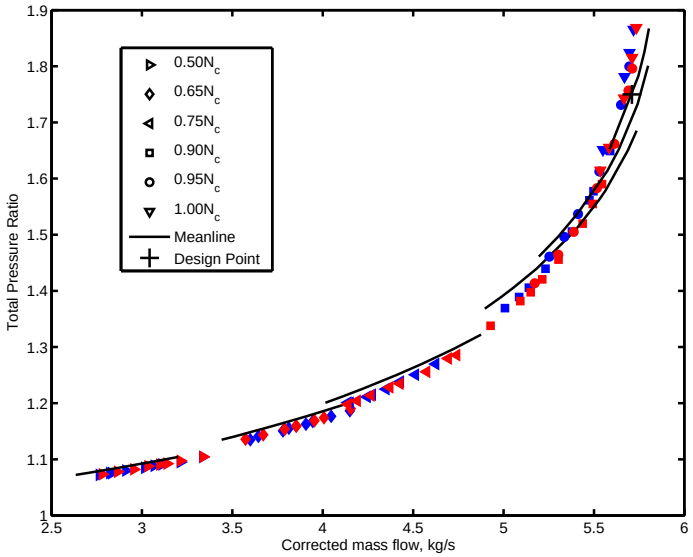

Figure 8. Measured and predicted total-to-total Pressure Ratio versus Corrected Mass Flow for ND-HiLT01 (Red: Tu=3.0%, Blue: Tu=5.5%).

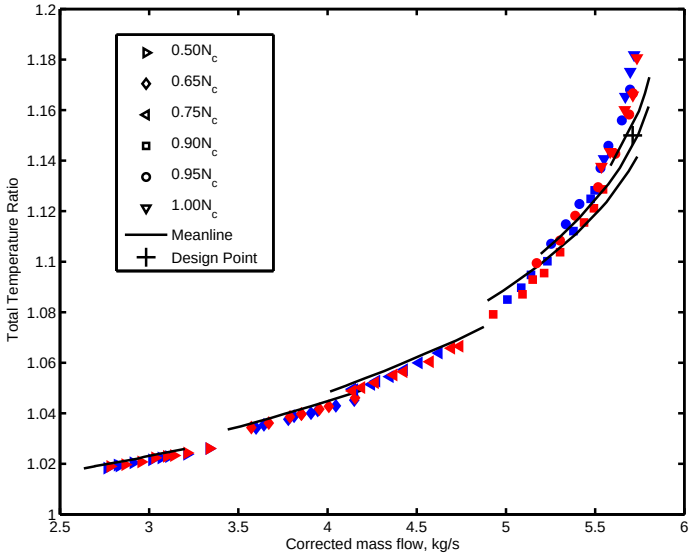

Figure 9. Measured and predicted total-to-total Temperature Ratio versus Corrected Mass Flow for ND-HiLT01 (Red: Tu=3.0%, Blue: Tu=5.5%).

from 0.21 to 0.89 for the experiments represented in Figs. 8-10. As expected from the PR and TR data, the efficiency was not sensitive to the FSTI, which further supports that the boundary layer transition and separation characteristics are insensitive to the Reynolds number. That is, a robust design was achieved with the design methods employed.

The efficiency at the higher speeds (0.90 - 1.00N_c) was found to be in the range $88\% < \eta < 92\%$. At 0.90N_c, 0.95N_c, and 1.00N_c there was a measurable difference in the efficiency trend lines between the two turbulence levels for the range of mass flow tested. The trend lines indicate that the increase in Tu resulted in an average increase of 0.5% in measured stage efficiency.

The meanline off-design trends are included in Fig. 10 as solid black lines. A single solid black symbol is included at the three highest speeds to differentiate the speed represented by each curve. The location of the symbol represents the design incidence location (note that the incidence is negative for all mass flows tested at the lower speeds). The overall efficiency of the turbine is well predicted by the meanline analysis. The slope of the trends lines were consistent with the slopes of the meanline predictions for each speed respectively. The meanline predictions matched the higher Tu level results for 0.90N_c and 0.95N_c. The lower Tu level at 1.00N_c was consistent with the meanline prediction for that speed.

Lastly, the results from both steady 3D CFD as well as time averaged solutions from the unsteady CFD solver are shown in Fig. 10. Note however, that the actual efficiency provided by the CFD was found to be lower than the measured values by about one percent. Hence, the CFD results were plotted as delta efficiencies from the design-point level, and hence these results are only valuable in the context of the slope of the efficiency with pressure ratio (i.e., incidence). It can be observed that the CFD does in fact predict this sensitivity very well, with the slope of the CFD results nearly matching the experimental data obtained with 3.0% turbulence intensity. Note that the numerical solutions used 1.0% FSTI as an inlet boundary condition, and was a design-level prediction of the results as opposed to postdiction.

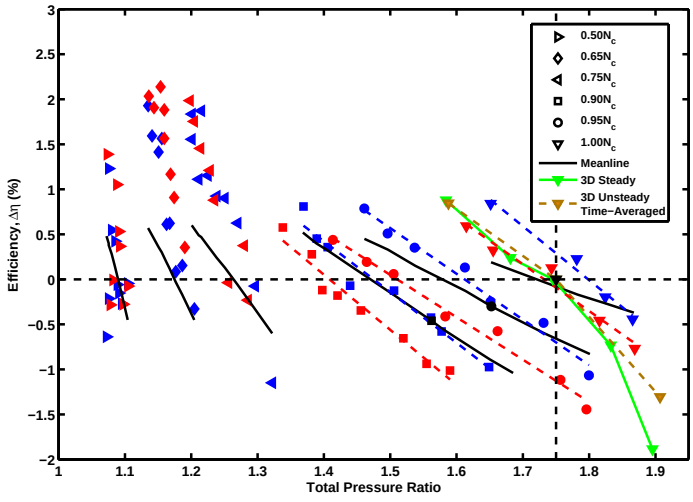

Figure 10. ND-HiLT01 measured and predicted design and off-design stage efficiency characteristics (Red: Tu=3.0%, Blue: Tu=5.5%).

The efficiency is shown as a function of the blade span at the design speed and mass flow rate in Fig. 11. There was no adjustment made to the absolute efficiency values from the CFD predictions. Spanwise efficiency was calculated by first averaging the inlet total temperature and pressure, and then using the individual spanwise measurements to calculate efficiency. The experimental data from both FSTI cases are shown from the individual exit probes. The numerical solution is shown as a single connected curve. The measured efficiency levels are within $\pm 1.0\%$ of the CFD result between 20% and 75% span. This agreement in the mid-span region is important because it validates the effectiveness of the boundary layer transition modeling used in the design phase of the ND-HiLT01.

The most obvious deviation from the data occurred in the ID and OD regions. This is consistent with the findings of Praisner et al. [20], in that the CFD simulations prove to be inaccurate at predicting the effect of secondary losses on efficiency. The secondary flows of highly loaded LP turbines are most likely very dependent on geometry and loading level. More work to understand the flow details will be needed before accurate physics based predictions can be made.

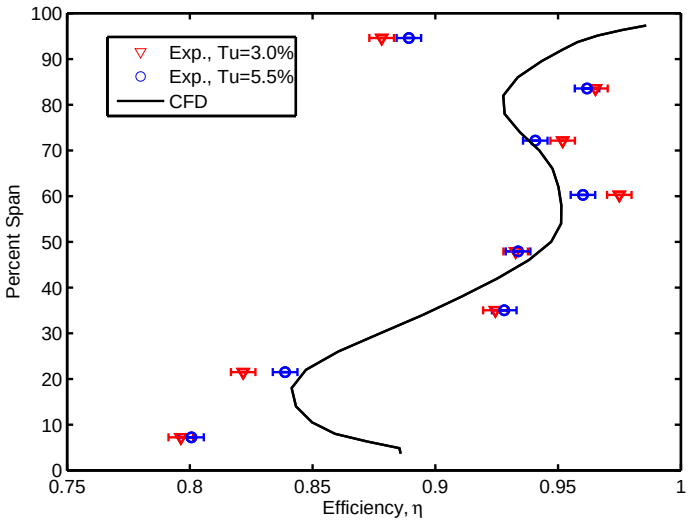

Figure 11. ND-HiLT01 efficiency versus span data at design condition with 3D RANS steady CFD prediction

The final metric for comparison of the experiment to the CFD is the absolute outlet flow angle. This is shown as a function of span in Fig. 12. The measurements were conducted using a cylindrical probe with two pressure taps with 90 degree separation. The flow angle was found by rotating the probe about its axis until the pressure differential was zero, indicating locally symmetric flow around the cylinder. The measured flow angles have an estimated uncertainty of ± 0.5 deg.

The outer 60% (40% to 100%) of the span was found to agree with the CFD prediction to within ± 2 degrees. The agreement with the data near the outer part of the span suggests that the net turning angle of the flow is well predicted at this location despite the over prediction of the efficiency near the blade tip. At the lower span values (near the hub) the absolute angle was over predicted, suggesting that the CFD was predicting more overturning than what was observed in the experiment.

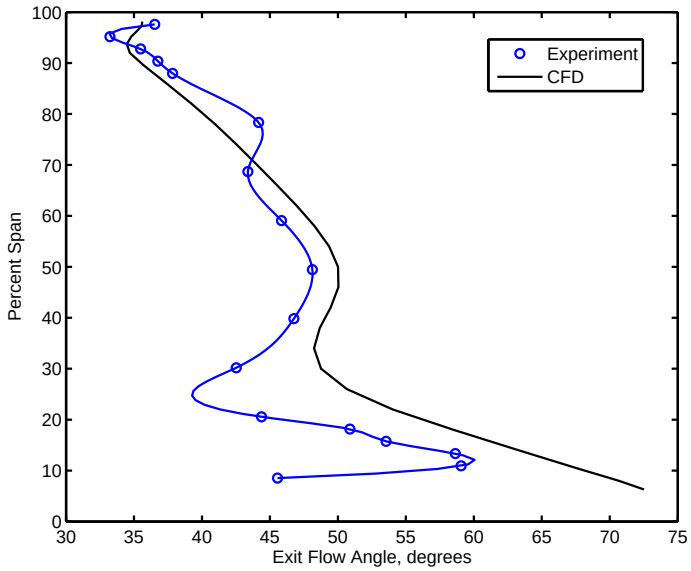

Figure 12. ND-HiLT01 measured (Tu=5.5%) and predicted outlet flow angle

DETAILED FLOW PHYSICS

The results of the 3D RANS solver of Ni [31] were used to study the detailed flow physics of the ND-HiLT01 vane and blade. The time-mean local Mach number contours in the relative frame of reference for the vane and blade rows at a condition near-design in terms of both corrected speed and pressure ratio are shown in Fig. 13. The nozzle surface boundary layers and exit wakes are thin and the wake trajectories suggest nearly zero exit angle deviation.

The relative Mach number contours for the blade row are shown on the right hand side of Fig 13. These data are best interpreted along with the time-averaged surface pressure distribution, which are shown as solid lines in Fig 14 for the same spanwise location. A rapid decrease in the suction side static pressure was evident on the suction surface over the first 20% of axial chord, with a concomitant acceleration to transonic flow. The static pressure on the suction surface and near-surface Mach

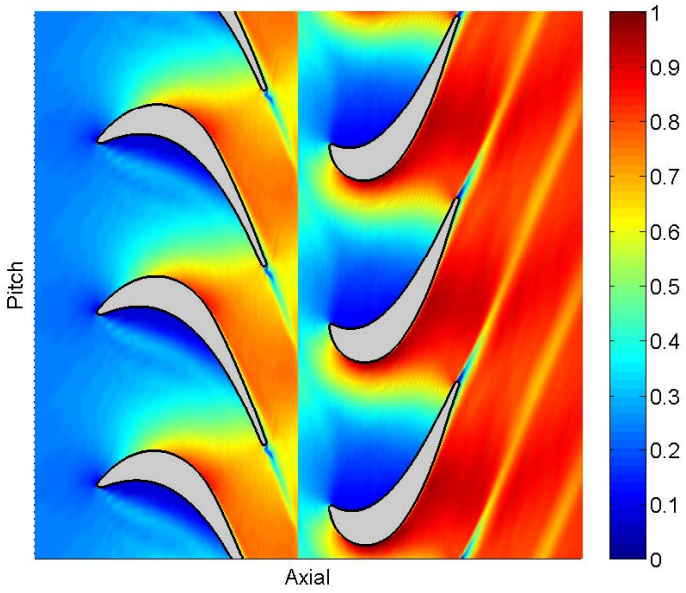

Figure 13. Time-mean Mach number contours at 74% span at 99% design speed and a total-to-total pressure ratio of 1.75.

number were observed to be nearly constant from 20% to 80% of axial chord. Note that there was no sharp local minima in the suction side pressure distribution, and the pressure is roughly constant over the uncovered portion of suction surface from 60% to 80% of axial chord. At higher pressure ratios, there is a deceleration of the flow downstream of the point of minimum pressure that is associated with a weak cross-passage shock wave. The suction side pressure did increase gradually to the trailing edge, and was accompanied by some boundary layer growth. This lead to a deviation angle of 1.7 degrees, but no flow separation.

The pressure side passage Mach number was less than 0.2 for 50% of blade pitch, with a mean pressure distribution that was nearly uniform over the first 60% of axial chord. Near the trailing edge of the turbine the flow was observed to be transonic over the entire throat, which is in agreement with the large slope observed in Fig. 8 and 9 at high corrected flow suggesting choked flow.

The peak-to-peak unsteady surface pressure is shown in Fig 14 as dashed lines around the mean pressure data. A Fourier analysis of the time series indicated that over 95% of the RMS of the unsteady pressure was found at the vane-passing frequency. Contours of the unsteady loading evaluated at this frequency are shown in Fig. 15 for both the pressure and suction sides of the airfoil. The largest contribution to the unsteady loading was found on the suction side of the airfoil near the outer half of the span, and between 20% and 30% of axial chord. Additional analysis using space-time correlations of the surface pressure indicated that the disturbances that led to the unsteadiness traveled with a

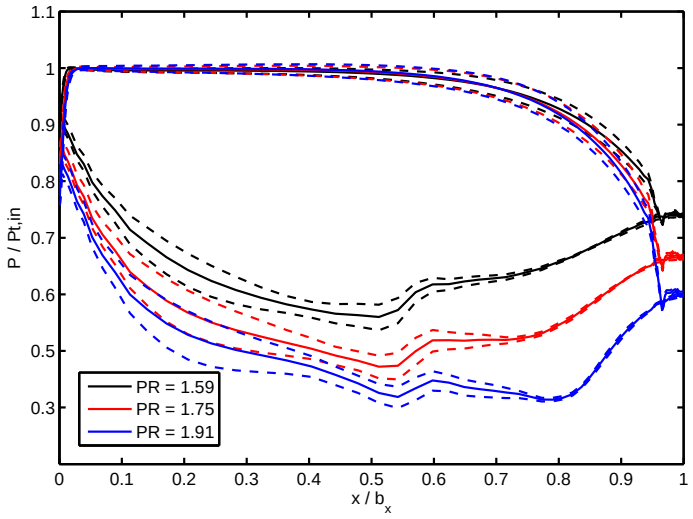

Figure 14. Unsteady loading variations at 99% speed. Solid lines are time-mean variations and dashed lines are peak-to-peak variations over 2 vane passings at 74% span on the blade.

time scale proportional to the fluid convection speed. This further suggests that the unsteadiness was simply wake passing, and not a compressible (i.e., acoustic or shock-induced) effect.

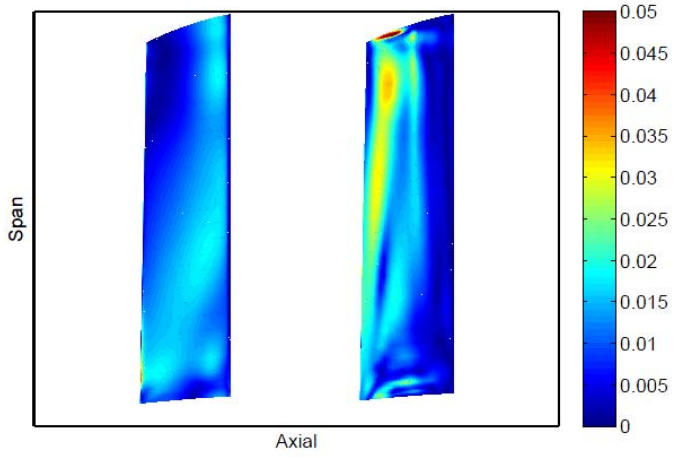

Figure 15. Unsteady pressure magnitudes normalized by stage-inlet total pressure at the fundamental upstream vane-passing frequency (L: Pressure side, R: Suction side.

Contours of time-resolved increase in entropy over stage inlet conditions are shown in Fig. 16 which illustrate the wake interactions with the rotor blades. These results show how the losses generated in the vane and blade rows are distributed at one instant. The vane wakes were observed to convect into the

rotor and become distorted and diffused as the flow accelerates through the throat. The suction side boundary layer is the largest contribution to the losses. The majority of entropy was generated very near the trailing edge on the blade suction surface. The high entropy fluid entered the wake, and was found to mix very slowly downstream of the rotor airfoils.

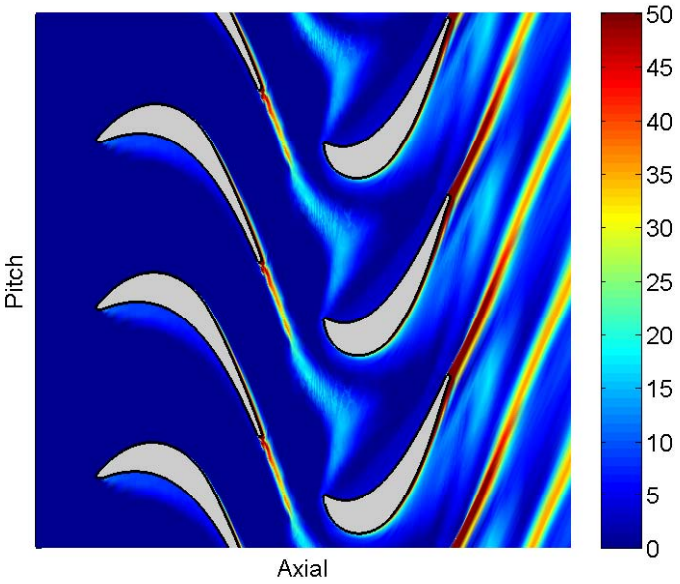

Figure 16. Time-resolved increase in local entropy over that at stage inlet (J/kg/K).

CONCLUSIONS

A transonic, highly loaded, low-pressure turbine stage (ND-HiLT01) was designed, and its performance and detailed flow physics were investigated both numerically and experimentally. The design process described assured that the turbine design was a true test of high-lift profile design philosophy to achieve acceptable performance at reduced part count/stage weight. Steady and unsteady numerical predictions were presented for design and off-design performance details.

The stage was studied experimentally in a recently constructed high-speed, continuous running, rotating turbine facility at the University of Notre Dame. Unique design features include the ability to control stage inlet temperature, nozzle only flow studies, and independent rotating sensor rings. The use of a magnetically levitated turbine rotor shaft coupled directly to a phase displacement torquemeter eliminated bearing resistance estimations typically associated with turbomachinery torque measurements.

The experimental results confirmed the ability of the design process presented to produce a relevant high-load LP turbine with acceptable design performance characteristics. In addition, the numerical modeling techniques of Praisner and Clark [19] were also able to accurately predict the design and off-design performance trends. This performance was realized without the addition of any passive or active form of flow control.

The stage was found to be relatively insensitive to Reynolds and Mach number over the range of tested variables. The effect of increasing FSTI from 3% to 5.5% was negligible for all speeds below $0.75N_c$ and resulted in an overall increase in efficiency of $\sim 0.5\%$ at speeds above $0.90N_c$ for the range of incidence angles. Experimental results confirm the blade surface flow is attached for the range of test conditions, even for positive blade incidence at design speed. In addition, other conditions suggested by the experimental data (e.g. choked rotor flow, overturning at the hub, wake effects) were confirmed by the numerical investigations.

The results presented imply that the aerodynamic efficiency of a high-load design is wholely dependent on the analytical competency of the design process, and not arbitrary limitations on loading levels. A rigorous physics-based design process was shown to produce a stage geometry which met predicted performance characteristics. Deficiencies still exist when modeling endwall and secondary flows. Further work is required to develop accurate models which predict the complex flow properties associated with these regions.

ACKNOWLEDGMENT

Special thanks to Mr. Frank Huber, Dr. Dan Dorney, and Dr. Bob Ni for guidance and advice on the use of their analysis systems. Mr. Huber's meanline code and Dr. Dorney's unsteady RANS solver were essential to guiding the design of the successful turbine stage, and the encouragement they provided in the early going of this work is gratefully acknowledged. Also, Dr. Ni's expertise and enthusiasm for the analysis of turbomachinery flows was especially important to the understanding of the off-design performance of the turbine.

REFERENCES

[1] Hodson, H., Huntsman, I., and Steele, A. B., 1994. "An investigation of boundary layer development in a multistage lp turbine". *J. of Turbomachinery,* ***116***, pp. 375–383.

[2] Curtis, E. M., Hodson, H. P., Banieghbal, M. R., Denton, J. D., Howell, R. J., and Harvey, N. W., 1997. "Development of blade profiles for low-pressure turbine applications". *J. of Turbomachinery,* ***119***, pp. 531–538.

[3] Prasiner, T., Grover, E., Knezevici, D. C., Popovic, I., Sjolander, S. A., Clark, J. P., and Sondergaard, R., 2007.

"Toward the expansion of low-pressure-turbine airfoil design space". In GT2008-27537.

[4] LaGraff, J. E., and Ashpis, D. E., eds., 2001. Minnowbrook III: 2000 Workshop on Boundary Layer Transition and Unsteady Aspects of Turbomachinery Flows, NASA/CP-2001-210888, NASA.

[5] Hourmouziadis, J., 1984. "Aerodynamic design of low pressure turbines". In AGARD-LS-167 Blading Desing for Axial Turbomachines.

[6] Hoheisel, H., Kiock, R., Lichtfuss, H. J., and Fottner, L., 1987. "Influence of free-stream turbulence and blade pressure gradient on boundary layer and loss behavior of turbine cascades". *J. of Turbomachinery,* ***109***, pp. 210–219.

[7] Vera, M., Zhang, X. F., Hodson, H. P., and Harvey, N. W., 2005. "Separation and transition control on an aft-loaded ultra-high-lift lp turbine blade at low reynolds number: high-speed investigation". In GT2005-68893.

[8] Stadmuller, P., and Fottner, L., 2001. "A test case for the numerical investigation of wake passing effects on a highly loaded lp turbine cascade blade". In 2001-GT-0311.

[9] Haselbach, F., Schiffer, H. P., Horsman, M., Dressen, S., Harvey, N. W., and Read, S., 2001. "The application of ultra-high lift blading in the br715 lp turbine". In ASME 2001-GT-0436.

[10] Gier, J., and Ardey, S., 2001. "On the impact of blade count reduction on aerodynamic performance and loss generation in a three-stage lp turbine". In 2001-GT-0197.

[11] Prakash, C., Cherry, D. G., Shin, H. W., Machnaim, J., Dailey, L., Beacock, R., Halstead, D., Wadia, A. R., Guillot, S., and Ng, W. F., 2008. "Effect of loading level and distribution on lpt losses". In GT2008-50052.

[12] Evans, D. C., and Wolfmeyer, G. W., 1972. "Highly loaded multi-stage fan drive turbine-plain blade configuration design". In NASA-CR-1964.

[13] Cherry, D. G., and Dengler, R. P., 1972. "The aerodyanamic design and performance of the NASA/GE E^3 low pressure turbine". In AIAA Paper No.1984-1126.

[14] Bons, J. P., Hansen, L. C., Clark, J. P., Koch, P. J., and Sondergaard, R., 2005. "Designing lp turbine blades with integrated flow control". In GT2005-68962.

[15] Coull, J. D., Thomas, R. L., and Hodson, H. P., 2008. "Velocity distribution for low pressure turbines". In GT2008-50589.

[16] Gier, J., Franke, M., Hubner, N., and Schroder, T., 2008. "Designing lp turbines for optimized airfoil lift". In GT2008-51101.

[17] Norris, G., 2009. "Upgrade promise: Product improvements should bring the trent 1000 close to spec before 787 tests". *Aviation Week and Space Technology,* ***170***(14), Apr 06, p. 36.

[18] Norris, G., 2009. "Turbine upgrade". *Aviation Week and Space Technology,* ***170***(18), May 04, pp. 44–45.

[19] Praisner, T. J., and Clark, J. P., 2007. "Predicting transition in turbomachinery - part 1: a review and new model development". *J. of Turbomachinery,* ***129***, pp. 1–13.

[20] Praisner, T. J., Grover, E. A., Rice, M. J., and Clark, J. P., 2007. "Predicting transition in turbomachinery - part 2: model validation and benchmarking". *J. of Turbomachinery,* ***129***, pp. 14–22.

[21] Clark, J. P., Koch, P. J., Ooten, M. K., Johnson, J. J., Dagg, J., McQuilling, M. W., Huber, F., and Johnson, P. D., 2009. Design of Turbine Components to Answer Research Questions in Unsteady Aerodynamics and Heat Transfer. Tech. Rep. AFRL-RZ-WP-TR-2009-2180, AFRL.

[22] Casey, M. V., 1994. "Computational methods for preliminary design and geometry definition in turbomachinery". In AGARD Lectures Series 195, in Turbomachinery design using CFD, pp. 1–1:1–22.

[23] Dorney, D. J., and Davis, R. L., 1992. "Navier-stokes analysis of turbine blade heat transfer and performance". *Journal of Turbomachinery,* ***114***, pp. 795–806.

[24] Vanderplaats, G. N., 1984. *Numerical Optimization Techniques for Engineering Design: With Applications*. McGraw-Hill, New York.

[25] Santner, T. J., Williams, B. J., and Notz, W. I., 2003. *The Design and Analysis of Computer Experiments*. Springer-Verlag, New York.

[26] Gross, A., and Fasel, H. F., 2007. "Investigation of low pressure turbine separation control". In AIAA 2007-520.

[27] Bons, J. P., Reimann, D., and Bloxham, M., 2008. "Separated flow transition on an lp turbine blade with pulsed flow control". *Journal of Turbomachinery,* ***130***, pp. 021014–1–021014–8.

[28] Bons, J. P., Pluim, J., Gompertz, K., Bloxham, M., and Clark, J. P., 2008. "The application of flow control to an aft-loaded low pressure turbine cascade with unsteady wakes". In GT2008-50864.

[29] McQuilling, M., 2007. "Design and validation of a high-lift low-pressure turbine blade". PhD thesis, Wright State University.

[30] Durschmidt, D. F., Medlock, A., and Miller, M. J., 2008. "An integrated design system for fans, compressors, and turbines: Part 3 - fan and compressor airfoil geometry generators". In GT2004-53633.

[31] Ni, R. H., 2009. *Aerodynamic Solutions Technical Reference Manual*. Aerodynamics Solutions, Inc., Manchester, CT.

[32] Ni, R. H., 1999. "Advanced modeling techniques for new commercial engines". In XIV ISOABE Conference. Florence, Itlay.

[33] Lax, P. D., and Wendroff, B., 1964. "Difference schemes for hyperbolic equations with high order accuracy". *Communications on Pure and Applied Mechanics,* ***17***, pp. 381–398.

[34] Law, C. H., and Puterbaugh, S. L., 1982. A Computer Program for Axial Compressor Design (UD0300M). Tech. Rep. AFWAL-TR-82-2074, AFRL.
[35] Ma, R., Morris, S. C., and Corke, T. C., 2006. "Design of a transonic research turbine facility". In AIAA 2006-1311.
[36] Bernard, P., and Wallace, J., 2002. *Turbulent Flow: Analysis, Measurement, and Prediction*. John Wiley and Sons, Inc., Hoboken, New Jersey.
[37] Langston, L. S., Nice, M. L., and Hooper, R. M., 1977. "Three-dimensional flow in a turbine cascade passage". *ASME Journal of Engineering for Power,* ***99***(1).